Tribology International 120 (2018) 243–254

Contents lists available at ScienceDirect

Tribology International

journal homepage: www.elsevier.com/locate/triboint

Effect of cylinder deactivation on tribological performance of piston compression ring and connecting rod bearing

N. Morris [a], M. Mohammadpour [a], R. Rahmani [a,*], P.M. Johns-Rahnejat [a], H. Rahnejat [a], D. Dowson [b]

[a] Wolfson School of Mechanical, Electrical and Manufacturing Engineering, Loughborough University, Leicestershire, UK
[b] School of Mechanical Engineering, University of Leeds, Leeds, UK

ARTICLE INFO

Keywords:
Cylinder deactivation
Piston compression ring
Big-end bearing
Friction
Power loss

ABSTRACT

Thermo-mixed-hydrodynamics of compression rings and big-end bearings are presented. Frictional losses under normal engine operating conditions for a gasoline engine and those with cylinder deactivation (CDA) are predicted. With CDA, the combustion chamber pressure increases in the active cylinders, whilst some residual pressure remains in the deactivated ones. For the former, the increased in-cylinder temperatures reduce viscous friction, whilst reducing the load carrying capacity, promoting increased boundary interactions. In deactivated cylinders, lower contact temperatures yield increased viscous friction. Overall, a 5% improvement in expended fuel is expected with the application of CDA. However, 10% of these gains are expended due to increased friction. The study demonstrates the need to consider total system effects when introducing new technologies such as CDA.

1. Introduction

Recent years have witnessed the emergence of new technologies for improved fuel efficiency of internal combustion engines. These include, but are not confined to, variable valve actuation (VVA), cylinder deactivation (CDA) and stop-start in congested traffic. CDA is one of the most widely adopted of these energy saving technologies. It varies the number of active cylinders to match the required engine capacity for a desired output power. Therefore, it is most suited to congested traffic or those instances where full engine power is not required. For example, in steady state highway driving when most of the parasitic losses can be attributed to pumping typically only 30–40% of the peak engine power would suffice.

As a result, significant improvement in fuel economy can be achieved for a host of manoeuvres using CDA, primarily because of improved volumetric fuel efficiency [1,2]. Sandford et al. [1] have shown that 20% fuel saving is attainable through the use of CDA.

Overall engine efficiency, given as: $\frac{BMEP}{QF_{A/F_a}} = \eta_f \eta_v \eta_m$, is typically a product of the indicated efficiencies; mechanical (η_m), volumetric (η_v) and fuel conversion (i.e. thermal) (η_f). It is commonly assumed that mechanical efficiency is independent of system-level changes which improve the volumetric and thermal efficiencies, such as the effect of CDA on frictional performance. As a result, the opportunity to harness the full potential of CDA is rather exaggerated as it disregards the performance of engine tribological conjunctions. Introduction of new technologies, such as CDA, affect the prevailing conditions in the load bearing conjunctions. In addition, the opportunity to refine the tribological conjunctions in order to mitigate any potential adverse effects is somewhat overlooked.

The main contributing factors determining the mechanical efficiency of an engine are pumping, windage and parasitic frictional losses; the last of which is the most significant. The investigation of frictional performance is the subject of the current paper.

Of the numerous bearing surfaces and seals within the internal combustion engine, the piston compression rings and the big-end bearings are the most susceptible to changes in the applied combustion process. During the traditional engine operating conditions (i.e. with all active cylinders; the standard operation mode), piston compression rings and big-end bearings have been shown to account for 5% of the expended input fuel energy [3].

The significant parasitic energy loss associated with the piston ring-cylinder liner conjunction has resulted in over 80 years of continuous research. The transient nature of piston operation with cyclic sliding velocity, loading and thermal conditions continues to pose significant challenges for time-efficient predictions and/or direct measurements of film thickness [4] and generated friction [5–7]. A comprehensive review

* Corresponding author.
E-mail address: R.Rahmani@lboro.ac.uk (R. Rahmani).

https://doi.org/10.1016/j.triboint.2017.12.045
Received 26 October 2017; Received in revised form 26 December 2017; Accepted 28 December 2017
Available online 2 January 2018

of lubricant film measurement techniques for ring-bore conjunctions is provided by Sherrington [8].

Early analyses included the works of Castleman [9], and Eilon and Saunder [10] who employed Reynolds equation in one dimension to obtain the film thickness at various discrete piston stroke positions. The results were somewhat optimistic, predicting the formation of a full hydrodynamic film throughout the engine cycle. Later, Furuhama [11] advanced the previous analyses with the inclusion of squeeze film lubrication, which can contribute to the retention of a thin, finite lubricant film at piston reversals, where there is no lubricant entrainment. Furthermore, the inclusion of squeeze film motion enables a transient analysis of lubrication conditions to be undertaken. Hamilton and Moore [12] employed the Swift [13] – Stieber [14] boundary conditions to include the effect of lubricant film depletion and rupture. Ruddy et al. [15] considered the influence of direct contact of contiguous surfaces with any diminution of lubricant film. They also included the effect of inter-ring gas pressures in their analysis. Dowson et al. [16] showed that a preceding ring would reduce the lubricant availability for those following behind in a ring-pack. It was shown that the resulting inlet starvation diminished the oil film thickness. It is now well-established that considerable boundary interactions occur at piston reversals between the compression and the power strokes [17,18]. In fact, Styles et al. [18] showed that frictional losses during this part of the piston cycle can account for more than 30% of the total losses. The prevailing conditions are also affected by the geometry of the ring contact face and its topography [19,20], as well as by the extent of ring-bore conformance during reversal [21,22].

Ring-bore conformance is also affected by elastodynamics of the ring, which is subjected to complex modal behaviour in its radial plane as well as in its out-of-plane motions. Analysis of these motions has been provided by Tian [23,24] showing their effects on wear and oil loss, and by Baker et al. [25–27] who included their effects on loss of sealing, ring jump and blow-by. In practice, compression ring-bore conformance is also affected by a *real* out-of-round cylinder bore as shown by the analysis of Rahmani et al. [28]. Any non-conformance of the ring to the surface of the cylinder liner can lead to loss of sealing with ensuing power loss and blow-by.

Loss of sealing also causes reduced friction which can cause ring jump and power loss as shown by Namazian and Heywood [29] and Baker et al. [27,30]. This power loss is caused by the flow of gasses through the cylinder-compression ring crevices, rather than through any generated friction. In fact, there is reduced friction with the ring jump phenomenon. Therefore, a balance between sealing function and excess friction in transition between mid-cycle compression and power stroke should be sought.

With CDA, the valves of the deactivated cylinders are closed with residual decreased cylinder pressures. With reduced pressure loading on the piston rings, there would be less direct boundary interaction of contiguous rough surfaces. However, due to the lack of combustion, the instantaneous lubricant temperature would be reduced, and an increased viscous friction would be expected because of higher lubricant viscosity at liner temperatures. Recent investigations, experimental and numerical, have all shown that the lubricant temperature is primarily governed by the cylinder liner temperature [31–34]. Viscous shear is the dominant mode of generated friction for most of the piston cycle as amply demonstrated by many authors [16–19,35,36]. Therefore, in-cylinder frictional losses are not necessarily reduced in the deactivated cylinders. In fact, the only reported study to date points to a contrary conclusion [37] in line with the foregoing discussions. However, the study in Ref. [37] was isothermal. A thermo-mixed hydrodynamic analysis is required, which is the subject of the current paper.

The other load bearing conjunction of interest is the connecting rod (big-end) bearing, which undergoes severe variations in dynamic loading. Martin and Booker [38] showed that the inertial loading has an appreciable effect on the film thickness. Later, Booker [39] developed a tribo-dynamic method, referred to as the Mobility Method, in order to tackle the dynamic effects in big-end bearings. The approach is detailed by Bodeo [40], together with its practical implications for prediction of conditions in big-end bearings. Bates et al. [41] also presented a theoretical model for dynamic loading of big-end bearings and validated it against experimental measurements. The effect of bearing bushing distortion upon the lubricant film thickness was neglected. The effect of localised deformation of a soft overlay on the bearing bushing was included by Rahnejat [42], who took into account inertial dynamics and gas pressure loading in a multi-body dynamics approach. Temperature rise has a significant effect on the film thickness of big-end bearings. Balakrishnan et al. [43] extended the work of Rahnejat [42] by adding the effect of shear heating for overlay crankshaft bearings. Mishra and Rahnejat [44] reported a thermo-elastohydrodynamic model for big-end bearings, including multi-lobed out-of-roundness of bearing bushing with different roughness patterns such as longitudinal, transverse, isotropic and anisotropic configurations. Wang et al. [45] included the effect of surface waviness of bearing bushing as a multi-lobe geometry, simulating the micro-features of the bearing.

Lubricant cavitation is a major issue in big-end bearings. Aside from cavitation erosion, it also affects the load carrying capacity and frictional performance. Bonneau et al. [46] provided a mass-conserving solution for bearings, which included the effect of structural deformation of the bearing bushing. A comprehensive multi-phase solution for journal bearings was provided by Shahmohamadi et al. [47], including the combined solution of Navier-Stokes, energy and vapour transport equations with modified Raleigh-Plesset equation for finite thin film flow conjunctions. Their numerical analysis was validated by experimental results and then extended to the case of big-end bearings subjected to CDA for a 4-cylinder engine. The predictions showed reduced brake specific fuel efficiency because of the increased frictional losses. The findings agreed with an earlier work reported by Mohammadpour et al. [48], who used a solution for the same engine configuration using Reynolds equation with Swift-Stieber boundary conditions, as well as the energy equation.

This paper provides solutions for a typical cylinder of a 4-cylinder engine, including both the top compression ring-liner conjunction and the big-end bearing with CDA. This integrated approach has not hitherto been reported in the literature.

2. Analysis methodology for piston ring

2.1. Hydrodynamics

To accurately evaluate the frictional power loss from compression ring-liner conjunction a mixed thermo-hydrodynamic analysis is required. The methodology used here is based on the one-dimensional approach presented by Morris et al. [20], where the average flow Reynolds equation is given as [49]:

$$\frac{\partial}{\partial x}\left(\frac{\varphi_x h^3}{12\eta_e}\frac{\partial \overline{p}}{\partial x}\right) = U\varphi_c\frac{\partial h}{\partial x} + \sigma\frac{\Delta U}{2}\varphi_s\frac{\partial h}{\partial x} + \varphi_c\frac{\partial h}{\partial t} \tag{1}$$

where, σ is the composite root mean square (RMS) roughness of the contiguous contacting surfaces and $\varphi_x, \varphi_s, \varphi_c$ are the pressure, shear and contact flow factors respectively, as defined by Patir and Cheng [49] and Chengwei et al. [50] (Appendix 1). The use of a one-dimensional Reynolds equation is justified because the peripheral ring length-to-contact width ratio in this case exceeds 30, as demonstrated by Haddad and Tjan [51]. An implication of this is that a fully conforming ring to the surface of an idealised right circular cylinder is assumed. The film thickness at any axial position along the ring contact face-width is given as:

$$h(x,t) = h_0(t) + s(x) \tag{2}$$

The contact frictional power loss and the elevated flash temperature of the surfaces require the inclusion of thermo-piezo-viscous behaviour of

the lubricant. In most piston compression ring contacts, the generated pressures are found to be insufficient to cause significant piezo-viscous behaviour of the lubricant, as well as any localised deformation of the contacting surfaces [17,19,22,35]. However, for the sake of completeness the piezo-viscous behaviour of the lubricant is included here, using Houpert's viscosity-pressure relationship [52]:

$$\eta_e = \eta_0 \exp\left\{(\ln\eta_0 + 9.67)\left(\left[\frac{\theta_e - 138}{\theta_0 - 138}\right]^{-s_0}\left[1 + 5.1\times10^{-9}(p - p_{atm})\right]^{Z} - 1\right)\right\} \tag{3}$$

where:

$$S_0 = \frac{\beta(\theta_0 - 138)}{\ln\eta_0 + 9.67},\ Z = \frac{\alpha}{5.1\times10^{-9}(\ln\eta_0 + 9.67)} \tag{4}$$

Lubricant density variation with pressure and temperature is included, using the modified Dowson and Higginson equation [53] to take into account the variation of lubricant density with temperature:

$$\rho = \rho_0\left(1 + \frac{0.6\times10^{-9}(p - p_{atm})}{1 + 1.7\times10^{-9}(p - p_{atm})}\right)\left[1 - 0.65\times10^{-3}(\theta_e - \theta_0)\right] \tag{5}$$

2.2. Boundary conditions

The current analysis assumes a drowned, fully flooded, inlet which extends to the edge of the ring contact face. However, in reality a starved inlet conjunction is likely due to restriction of oil flow through the ring pack.

The inlet pressure in the upstroke motion of the piston is considered to be the same as the combustion chamber pressure, whilst in the downstroke the inlet pressure is considered to be the crank case pressure. In a more precise approach, the actual inlet pressure during downstroke should be set to the inter-ring pressure (i.e. the pressure in the area between the compression and the scraper ring). This requires the inclusion of a gas blow-by model such as that reported in Refs. [27,54,55].

At the exit of the conjunction, Swift [13]-Stieber [14] exit boundary conditions are implemented as:

$$p = p_c,\quad \frac{dp}{dx} = 0 \text{ at } x = x_c \tag{6}$$

where, p_c is the cavitation vaporisation pressure of the lubricant at the location of lubricant film rupture.

The hydrodynamic load carrying capacity is then obtained as: $W_h = l\int_{-b/2}^{x_c} p dx$.

2.3. Friction and power loss

The average lubricant film hydrodynamic shear stress is:

$$\overline{\tau} = \pm\varphi_{fp}\frac{h}{2}\left(\frac{d\overline{p}}{dx}\right) - \frac{\eta_e \Delta U}{h}(\varphi_f \pm \varphi_{fs}) \tag{7}$$

where the positive and negative signs represent the ring and the liner surfaces respectively.Therefore, viscous friction becomes:

$$f_{vi} = \int_{-b/2}^{b/2}\overline{\tau}\, dA_v \tag{8}$$

where A_v is the area attributed to hydrodynamic action only, thus subjected to viscous shear.

During parts of the piston cycle where mixed regime of lubrication occurs, a proportion of the load is carried by opposing asperity pairs on the counter face surfaces. The generated asperity load resulting from these interactions is calculated using [56]:

$$W_a = \frac{8\sqrt{2}}{15}\pi(\zeta\kappa\sigma)^2\sqrt{\frac{\sigma}{\kappa}}E' A F_{5/2}(\lambda) \tag{9}$$

where, E' is the reduced (effective) Young's modulus of elasticity of the contacting pair, $\zeta\kappa\sigma$ is the roughness parameter, σ/κ is a measure of average asperity slope and $F_{5/2}$ is a statistical function for a surface whose uppermost region conforms to a Gaussian distribution of asperity heights. Its value can be evaluated as a function of the gap between the two contiguous surfaces using a 3rd or 5th-order polynomial fit as described in Refs. [33,34].

The contact reaction is: thus: $W = W_h + W_a$.Therefore, the actual contact area of asperity tips can be written as [56]:

$$A_a = \pi^2(\zeta\kappa\sigma)^2 A F_2(\lambda) \tag{10}$$

where F_2 is a statistical function and can be evaluated using curve fit polynomial equations [33,34]. In practice, the surface of the cylinder liner insert is cross-hatched and honed, with a non-Gaussian asperity height distribution as shown by Leighton et al. [57]. However, for run-in cylinder liners the assumption of a Gaussian distribution of uppermost roughness heights is reasonable.

A thin lubricant layer is assumed to be adsorbed or bonded to the counter face surfaces or retained in the interspatial valleys of interacting asperity pairs. This layer would act in non-Newtonian shear at the lubricant's Eyring shear stress, τ_0 [58]. Additionally, when the contiguous surfaces come into direct contact, the boundary shear strength of the softer of the counter face surfaces ς would contribute to friction. For ferrous surfaces: $\varsigma = 0.17$ [59]. Thus, the boundary component of friction becomes:

$$f_b = \tau_0 A_a + \varsigma W_a \tag{11}$$

Therefore, total friction is:

$$f = f_{vi} + f_b \tag{12}$$

2.4. Thermal model

A brief description of the thermal model, initially reported by Morris et al. [33], is provided here for the sake of completeness. The rate of frictional energy loss dissipated in the contact is obtained as:

$$P_r = \dot{Q} = f\Delta U \tag{13}$$

The contacting surfaces conduct the generated heat away. In addition, the generated heat can also be convected away by the lubricant film. A diagrammatic representation is provided in Fig. 1.

The model includes a set of defined thermal resistive barriers given as:

$$R_f = \frac{S_f}{k_s A},\ R_v = \frac{1}{h_t A}, R_l = \frac{h_0}{2k_l A},\ R_e = \frac{1}{\dot{m}c_p} \tag{14}$$

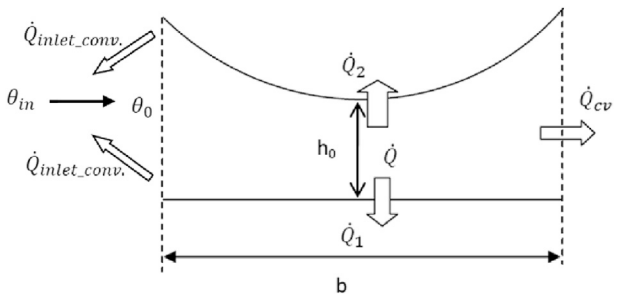

Fig. 1. Heat partition with the piston ring cylinder liner contact (Morris et al. [33]).

The thermal resistive barriers require the characteristic lengthS_f. For the cylinder liner the characteristic length is a function of the average contact transit time: $2b/\Delta U$. The solution provided by Sharif et al. [60] gives:

$$S_{f1} = \sqrt{\frac{2k_{s1}b}{\rho_{s1}c_{s1}\Delta U}} \tag{15}$$

Unlike the cylinder liner, the ring surface is always exposed to the heat source. When viewed as unwrapped, the rectangular surface characteristic length, S_{f2} can be stated as [61]:

$$S_{f2} = \frac{1}{\pi A}\left\{ bl^2 \sinh^{-1}\left(\frac{b}{l}\right) + lb^2 \sinh^{-1}\left(\frac{l}{b}\right) + \frac{1}{3}\left[l^3 + b^3 - \left(b^2 + l^2\right)^{3/2} \right] \right\} \tag{16}$$

A thermal resistance method, portrayed in Fig. 2, can be produced to determine the heat transfer through the bounding surfaces or that carried away by the lubricant film.

Thus, the average lubricant film temperature rise, used to calculate the effective viscosity, is given as:

$$\theta_e = \frac{\left(\dot{Q}R_e + \theta_0\right)\prod_{i=1}^{2} R_i + R_e \sum R_i \theta_{sj}}{\prod_{i=1}^{2} R_i + R_e \sum_{i=1}^{2} R_i}, \; i,j \in 1,2 \text{ and } i \neq j \tag{17}$$

where, i and j are indices related to the liner and ring surfaces. The temperature rise for each contacting surface is found through an iterative procedure as:

$$\Delta\theta_i = \frac{R_{fi}}{R_i}(\theta_e - \theta_{si}) \tag{18}$$

2.5. Method of solution

The solution procedure is as follows:

Step 1: The combined gas pressure loading and the elastic force due to ring tension can be calculated at any crank angle, ψ [28]:

$$F = F_e + F_g \tag{19}$$

where, F_e is the ring elastic tension which can be calculated using the elastic ring pressure given by: $P_e = \frac{GEI}{3\pi b r_0^4}$, and $F_g = 2\pi r_0 b P_g$ is the force generated by combustion gas, P_g, applied to the inner rim face of the ring. A more accurate account of gas pressure loading can be obtained through a gas blow-by analysis [27,54,55].

Step 2: The procedure is initialised with a guess for the minimum lubricant film thickness with ambient values used for lubricant viscosity and density, enabling the determination of hydrodynamic pressure distribution using equation (1).

Step 3: The Stribeck oil film ratio and the load share for any asperity contact are determined using equation (9).

Step 4: The nominal clearance (initial minimum film thickness) is adjusted using: $h_0^n = (1 + \varepsilon\chi)h_0^{n-1}$ where the numerical damping factor $\varepsilon \approx 0.075$ and χ is an adjusting parameter given as: $\chi = \frac{W(\psi) - F(\psi)}{\max\{W(\psi), F(\psi)\}}$ [62], until the contact reaction balances the applied load calculated in Step 1.

Step 5: Friction and power loss are calculated through the use of equations (8), (11) and (12). The frictional power loss is then used to determine the contact temperature rise.

Step 6: The temperature rise in the contact allows the calculation of effective lubricant viscosity and density using equations (3) and (5), which are then used to restart the process at Step 2.

Step 7: The following convergence criteria should be satisfied for generated pressures, load, and effective temperature at any crank angle respectively [28,62]:

$$e_p = \frac{\sum_{i=1}^{I}\sum_{j=1}^{J}\left|p_{i,j}^n - p_{i,j}^{n-1}\right|}{\sum_{i=1}^{I}\sum_{j=1}^{J} p_{i,j}^n} \leq 1 \times 10^{-6} \tag{20}$$

$$e_F = \frac{|F(\psi) - W(\psi)|}{F(\psi)} \leq 1 \times 10^{-3} \tag{21}$$

$$e_\theta = \frac{\left|\theta_e^n(\psi) - \theta_e^{n-1}(\psi)\right|}{\theta_e^n(\psi)} \leq 1 \times 10^{-4} \tag{22}$$

$$e_\psi = \frac{|h_0(\psi) - h_0(\psi - 720)|}{h_0(\psi - 720)} \leq 1 \times 10^{-3} \tag{23}$$

Step 9: When all the convergence criteria are met, the crank angle is updated and the procedure is repeated.

3. Analysis methodology for big-end bearing

Mohammadpour et al. [48] provided details of a big-end bearing analysis approach under CDA. The methodology used here is a condensed version of the same.

3.1. Elastohydrodynamic conjunction

For the case of a short-width big-end bearing with negligible side leakage, Reynolds equation in polar coordinates is:

$$\frac{\partial}{\partial z}\left(\frac{h^3}{\eta}\frac{\partial p}{\partial z}\right) = 6\left(\omega\frac{\partial h}{\partial \vartheta} + 2\frac{\partial h}{\partial t}\right) = 18\omega\frac{\partial h}{\partial \vartheta} \tag{24}$$

The film thickness for an elliptic bore bearing at any circumferential position is given as [48] (see Fig. 3):

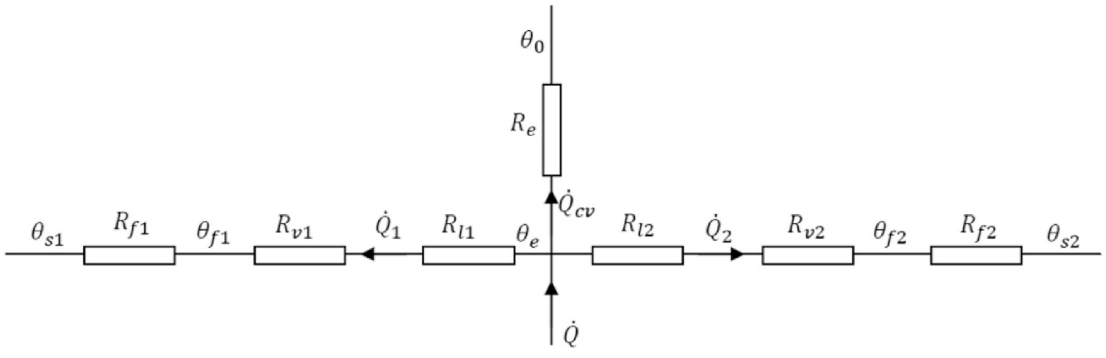

Fig. 2. Thermal resistance within the piston ring cylinder contact (Morris et al. [33]).

$$h(\vartheta) = \frac{ab}{\sqrt{a^2 \sin^2 \vartheta + b^2 \cos^2 \vartheta}} - r - x\cos\vartheta - y\sin\vartheta + \delta \tag{25}$$

where:

$$a = r + c_{min} \text{ and } b = r + c_{maj} \tag{26}$$

$x = e_0 \sin\varphi$ and $y = -e_0 \cos\varphi$ are the geometric eccentricities of the bushing and the journal centres with an eccentricity of e_0 and an attitude angle φ. δ is the elastic deformation of the soft bushing overlay such as a layer of Babbitt. The conformal nature of the contact and the relatively low elastic modulus of the overlay enable the determination of deflection using the column method [42]:

$$\delta = \frac{(1-2\upsilon)(1+\upsilon)d}{E(1-\upsilon)}p \tag{27}$$

where E and υ are Young's modulus and Poisson's ratio for the soft overlay and d is its thickness.

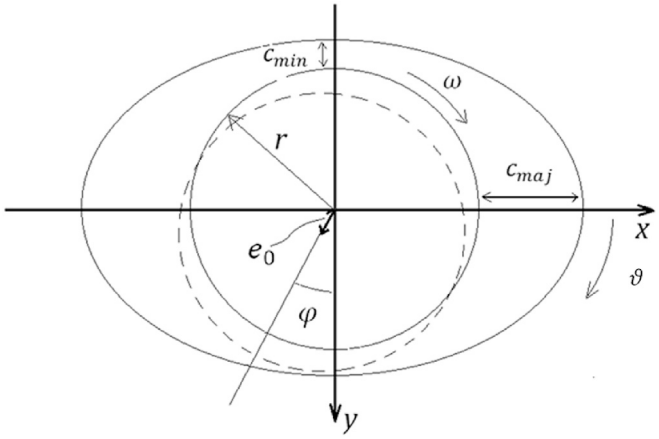

Fig. 3. Geometry of elliptic bore big-end bearing (Mohammadpour et al. [48]).

3.2. Frictional power loss

Viscous friction acting on the journal is obtained as:

$$f_{vi} = \int \left(h\frac{dp}{dz} + \frac{\eta}{h} r\omega \right) dA_v \tag{28}$$

The asperity contact area can be obtained using the Greenwood and Tripp model [56] already described by equation (9)–(11). Therefore, the total power loss for the big-end bearing becomes:

$$P_b = (f_{vi} + f_b) r\omega \tag{29}$$

3.3. Thermal model

The bearing analysis employs a similar heat partitioning model to that described previously. The difference is that the bushing and journal are continually exposed to the heat source so the characteristic length for both surfaces can be written as [61]:

$$S_{fi} = \frac{1}{2A}\left\{ (2\pi r)L^2 \sinh^{-1}\left(\frac{2\pi r}{L}\right) + L(2\pi r)^2 \sinh^{-1}\left(\frac{1}{2\pi r}\right) + \frac{1}{3}\left[L^3 + (2\pi r)^3 - \left(L^2 + (2\pi r)^2\right)^{3/2} \right] \right\} \tag{30}$$

3.4. Method of solution

The solution procedure is:

Step 1: At any crank angle, ψ, the instantaneous connecting rod angle, ϕ is obtained using equation (31) [63]. The applied bearing load is found using equation (32):

$$\cos\phi \approx 1 - \frac{r_c^2}{2l_c^2}\sin^2 \omega t \tag{31}$$

$$F = \frac{F_{in}}{\cos\phi} + F_G \tag{32}$$

where, F_{in} is the inertial loading generated by system dynamics [42]:

$$F_{in} = r_c\omega^2 m\left(\cos\omega t + \frac{r_c}{l_c}\cos 2\omega t\right) \tag{33}$$

The bearing load in terms of connecting rod obliquity angle is [42]:

$$F_G = \frac{p_g A_p}{\cos\phi} \tag{34}$$

Step 2: An initial guess is made for eccentricity, e_0 and generated pressures are obtained from equation (24).

Step 3: Lubricant rheological functions are updated from equations (3) and (25).

Step 4: Generated pressures cause localised deflection (equation (27)), thus the thickness of film and the load balance using the convergence criterion:

$$e_F = \frac{|F - W|}{F} \le 1 \times 10^{-3} \tag{35}$$

Step 5: The initial eccentricity is altered if the criterion is not met. Otherwise, the crank angle ψ is advanced. This procedure is repeated for the entire 4-strokes of the engine cycle until a cyclic convergence is achieved.

4. Engine specifications and input data

A typical 4-cylinder 4-stroke spark ignition c-class vehicle gasoline engine with a capacity of 1.4 L operating at 3000 rpm is considered in the current analysis. The combustion pressure for three possible in-cylinder operating conditions and the average cylinder liner temperature are measured and shown in Fig. 4. One condition refers to the engine operating under standard operating conditions, where all the four cylinders are active. Under CDA two redundant deactivated cylinders have reduced in-cylinder pressures and liner temperatures. The limited pressure variation is due to the compression and expansion of the residual combustion chamber content. The two active cylinders experience higher in-cylinder pressures in order to maintain the engine desired output power. This is accompanied by a rise in the cylinder liner temperature.

The engine geometric, material, lubricant and surface properties are listed in Tables 1–4. The cylinder liner is cross-hatch honed. Additional surface topographical parameters are provided in Table 4. The honing angle of 30° is used.

5. Results and discussion

5.1. Results and discussion: piston compression ring conjunction

The minimum lubricant film thickness separating the piston compression ring and the cylinder liner is shown in Fig. 5 for a complete 4-stroke engine cycle. Two engine operating conditions are presented; (i)- standard operation (with all active cylinders) and (ii)- with cylinder deactivation. These results are for a typical cylinder condition. Therefore, with cylinder deactivation the results are presented for both an active

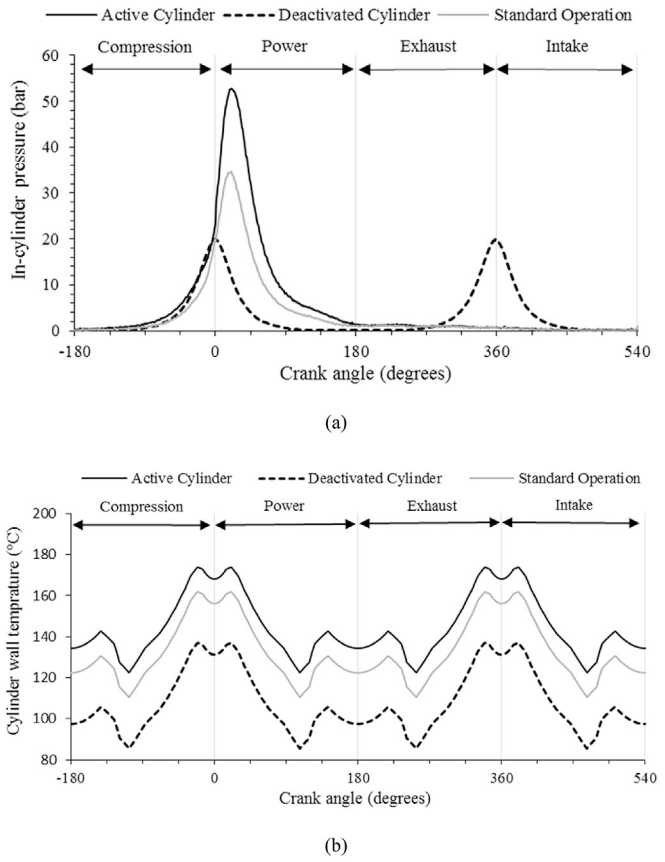

Fig. 4. Measured input data; (a) In-cylinder pressure, (b) Cylinder liner temperature.

Table 1
Lubricant data.

Parameter	Value	Unit
Lubricant density	849.7 @ 15 °C, 833.8 @ 40 °C	Kg m^{-3}
Kinematic viscosity	59.99 @ 40 °C, 9.59 @ 100 °C	$\times 10^{-6}$ m^2s^{-1}
Thermal conductivity	0.225 @ 120 °C	$Wm^{-1}K^{-1}$
Specific heat capacity	2360 @ 120 °C	$Jkg^{-1}K^{-1}$
Thermal expansion coefficient	6.5×10^{-4}	K^{-1}

Table 2
Engine geometry.

Parameter	Value	Unit
Pin radius, r_c	39.75	mm
Length of connecting rod, l_c	138.1	mm
Nominal bore radius, r_0	40.52	mm
Ring face-width, b	1.15	mm
Ring radial thickness, a	3.5	mm
Free ring end-gap, G	10.5	mm
Big-end bearing width, L	16.8	mm
Big-end bearing bushing radius, r	21.0	mm
Big-end bearing minor diametral clearance, C_{min}	20.0	μm
Big end bearing major diametral clearance, C_{max}	30.0	μm
Shell or soft overlay thickness, d	2.6	mm

and a deactivated cylinder. The demarcation line between a full hydrodynamic film and that resulting under mixed regime of lubrication, based on the Stribeck oil film ratio $\lambda = 3$, is also shown.

For all cases the film thickness diminishes with reduced lubricant entrainment when approaching piston reversals. In the vicinity of piston reversals, the applied load is almost entirely carried by squeeze film lubrication and any direct interaction of the opposing rough surfaces. At

Table 3
Material properties.

Parameter	Value	Unit
Liner material	Grey cast iron	–
Young's modulus of elasticity for liner material	92.30	GPa
Liner Poisson's ratio	0.211	–
Density for liner material	7200	kgm^{-3}
Thermal conductivity for liner material	55	$Wm^{-1}K^{-1}$
Specific heat capacity for liner material	460	$Jkg^{-1}K^{-1}$
Ring material	Steel SAE 9254	–
Modulus of elasticity for the ring material	203	GPa
Ring's Poisson's ratio	0.3	–
Ring coating	Chromium Nitride (CrN)	–
Modulus of elasticity for CrN	400	GPa
Poisson's ratio for CrN	0.2	–
Thermal conductivity of CrN	12.134	$Wm^{-1}K^{-1}$
Bearing overlay	Babbitt	–
Journal material	SG cast iron	–
Babbitt's Poisson's ratio	0.33	–
Babbitt's modulus of elasticity	60	GPa
Thermal conductivity for the bushing	46	$Wm^{-1}K^{-1}$
Thermal conductivity of journal	25.96	$Wm^{-1}K^{-1}$

Table 4
Surface roughness parameters.

Parameter	Value	Unit
Ra of liner surface plateau	0.26	μm
Rk of liner (plateau height)	0.75	μm
Rpk of liner plateau	<0.3	μm
Rvk (liner grooves)	>0.3	μm
Ra of ring contact surface	0.235	μm
Roughness parameter ($\zeta\kappa\sigma$)	0.04	–
Measured asperity gradient (σ/κ)	0.001	–
Big-end bearing composite surface roughness	1	μm

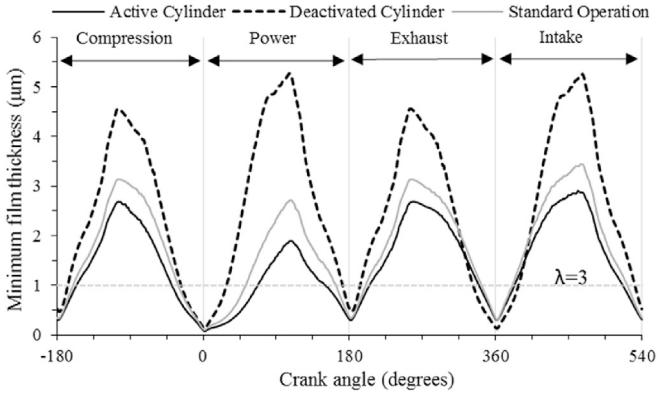

Fig. 5. Piston compression ring minimum film thickness.

mid-stroke the film thickness varies mainly in accord with lubricant dynamic viscosity which is largely dependent on the cylinder liner temperature. In the deactivated cylinder the reduced liner temperature leads to an increased film thickness. Likewise, the higher cylinder liner temperatures in the active cylinders reduce the viscous load carrying capacity.

Fig. 6 shows the predicted generated friction during a full 4-stroke engine cycle. Boundary and viscous friction are clearly observed. At mid-stroke the slope of friction follows the viscous service parameter: $(\Delta U\eta/h)$, whilst at the reversals, when the rough contiguous surfaces come into contact, there is a sharp rise in generated friction. Comparison of Figs. 5 and 6 is instructive in observing the influence of regime of lubrication on frictional performance. As well as the primary friction peak experienced in all operational conditions between the crank angles:

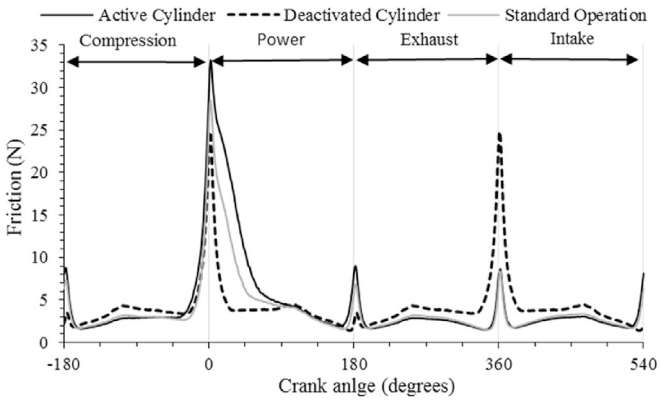

Fig. 6. Piston compression ring friction.

$-10° < \psi < 90°$, corresponding to compression to mid power strokes, a second friction peak is observed in the deactivated cylinder in the region: $350° < \psi < 370°$. The significant boundary friction observed in this region is as the result of elevated in-cylinder pressures (Fig. 4a) and the contact load due to the compression of the residual combustion chamber content.

The corresponding frictional power losses for each of the cases studied are shown in Fig. 7. The most significant power losses are concentrated at mid-stroke, where the sliding velocity attains its maximum value. The deactivated cylinder experiences significant power loss at mid-stroke as the result of a lower cylinder liner temperature, corresponding to a higher lubricant viscosity. The highest power losses occur during the power stroke as the high contact loads promote a mixed regime of lubrication for a longer duration. It is noteworthy that the power loss in the deactivated cylinder is very similar to the standard engine operating conditions. This, together with the fact that active cylinders of a CDA arrangement are subjected to higher combustion pressures, show that CDA promotes deteriorating in-cylinder frictional power loss. To a certain extent this offsets the envisaged gains through fuel saving made by deactivation of some of the cylinders.

5.2. Results and discussion: big-end bearing conjunction

Fig. 8 shows the predicted minimum film thickness variation of the big-end bearing through a full engine cycle. The results show that the film thickness reduces critically in the case of active cylinders with CDA. The dashed-line in the figure shows the onset of mixed regime of lubrication after which some boundary friction contribution ensues. The bearing of a deactivated cylinder carries lighter loads, allowing for significantly higher film thickness during the power stroke. However, the deactivated cylinder experiences increased loading in the exhaust and

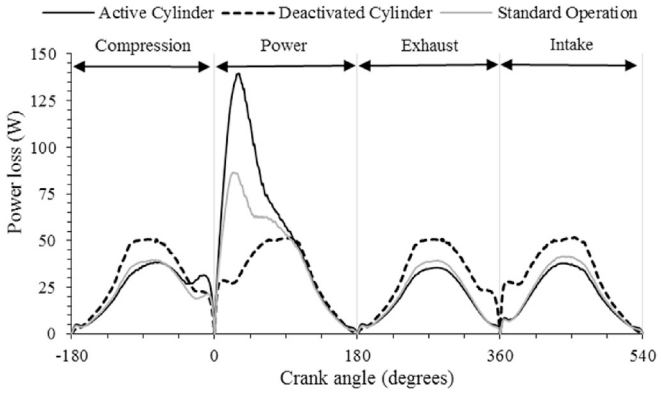

Fig. 7. Piston compression ring power loss.

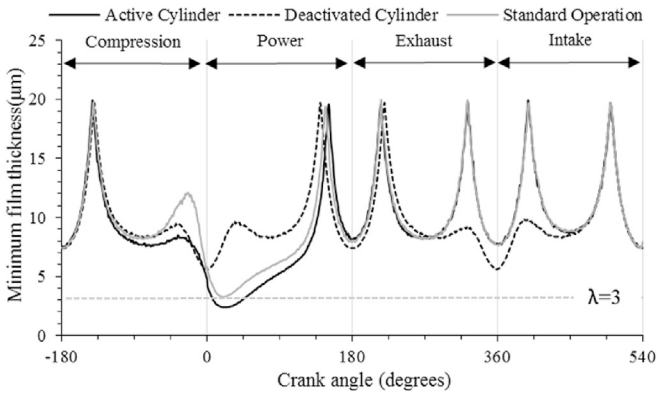

Fig. 8. Big-end bearing minimum film thickness.

intake strokes, causing a reduced bearing lubricant film thickness.

The frictional power loss in the various big-end bearing conjunctions is shown in Fig. 9. A significant rise in boundary friction is observed during the power stroke as would be expected. Under standard operating conditions a small rise in friction can be observed because a reduction in film thickness increases the lubricant film shear rate. During the other strokes there is little difference between the various operating conditions.

6. Concluding remarks

The average power loss across the whole engine cycle for both the compression ring and big-end bearing conjunctions are presented in Fig. 10. It can be observed that for both contacts a significant increase in power loss occurs as a result of cylinder deactivation. This has been

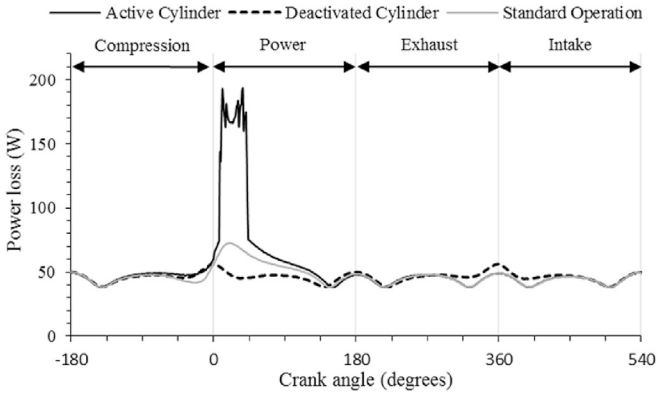

Fig. 9. Big-end bearing power loss.

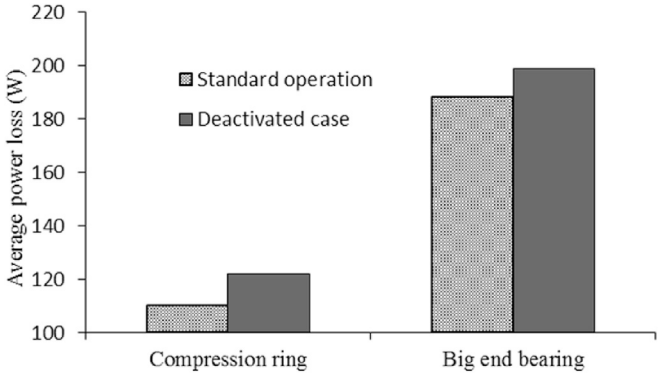

Fig. 10. Piston ring-cylinder liner and big-end bearing power loss.

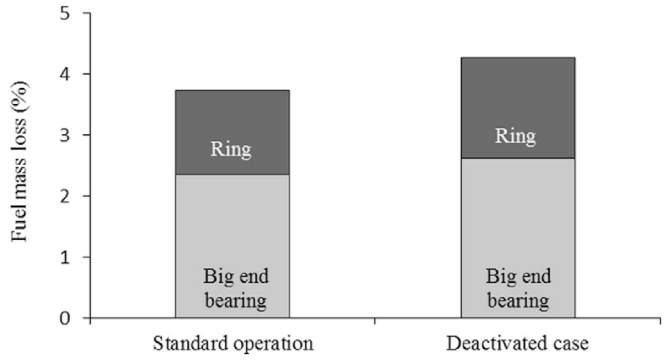

Fig. 11. Fuel lost from piston ring cylinder liner and big end bearing friction.

shown to be due to the changes in the cylinder liner temperature and an increase in loading for the cylinders which remain active. Most significantly, during cylinder deactivation the big-end bearing of an active cylinder is shown to operate in a mixed regime of lubrication. This can be remedied through appropriate bearing design. A second key observation is that the lower cylinder liner temperatures in deactivated cylinders promote higher losses due to shear in the piston ring conjunction. Increased loading of the piston ring-cylinder liner contact in the active cylinder with CDA dramatically increases the frictional power loss. Palliative measures such as surface texturing of the piston ring [64–66] or the cylinder liner at the top dead centre reversal [67] can reduce this problem to a certain extent.

It is instructive to represent the effect of frictional power losses in the form of approximate mass of fuel expended for each operational scenario; (a)- full engine operation and (b)- the alternative CDA configuration. The calculations are included in Appendix 2. The results are presented in Fig. 11. A 0.5% increase in input fuel expended due to friction at the two investigated conjunctions is predicted. Under standard operating conditions the piston compression ring and the big-end bearing frictional losses are shown to account for 1.37% and 2.35% of the input fuel mass respectively. With cylinder deactivation, the piston compression ring and the big-end bearing frictional losses account for 1.65% and 2.61% of the input fuel mass respectively. The analysis presented here is confined to the case of cylinder compression rings and big-end bearings. These are directly affected by the changes in the in-cylinder conditions. However, this is also true for piston skirt-cylinder liner conjunction, which with modern partially-skirted pistons undergoes significant thermo-elastic distortion, affecting the conjunctional gap [70,71]. Therefore, any changes in cylinder pressure as the result of CDA and the ensuing cylinder temperature also alter the engine fuel efficiency, which should be studied, but is outside the scope of the current paper. The only other contact conjunction of note is the cam-follower, which owing to the prevalent elastohydrodynamic regime of lubrication (EHL) only accounts for 6% of the frictional losses (a fraction of the expended fuel). As the output power is maintained with CDA, the contact sliding speed, the dominant parameter for the EHL, would remain almost unchanged.

There are some practical implications of the analysis results, indicating that selection of suitable ring and/or liner coating material and bearing overlay can improve upon heat conduction from these contacts, thus improving upon lubrication conditions and reducing the frictional power losses.

Acknowledgments

The authors would like to express their gratitude to the UK Engineering and Physical Sciences Research Council (EPSRC) (EP/G012334/1) for the financial support of the Encyclopaedic Program Grant (www.Encyclopaedic.org), under which the majority of this research was carried out.

Nomenclature

A	Apparent contact area
A_a	Asperity contact area
A_v	Area subjected to viscous shear
A_p	Area of piston head
a	Ring radial thickness
b	Ring axial-width (contact face-width)
c_{maj}	Contact clearance along the semi-major axis
c_{min}	Contact clearance along the semi-minor axis
c_p	Specific heat capacity of the lubricant
c_s	Specific heat capacity of solid surfaces
d	Thickness of bushing shell or overlay
e_0	Journal/Bushing eccentricity
e_F	Error tolerance for load convergence
e_p	Error tolerance for pressure convergence
e_θ	Error tolerance for temperature convergence
e_ψ	Error tolerance for crank angle periodicity
E	Young's modulus of elasticity
E'	Reduced (effective) elastic modulus of the contacting pair
F	Total contact applied load
$F_{5/2}, F_2$	Statistical functions
F_A	Air-fuel mass ratio
F_e	Ring tension force
F_{in}	Inertial imbalance force
F_G	In-cylinder gas force
F_g	Combustion gas force applied to the ring
f	Friction
f_b	Boundary friction

f_{vi}	Viscous friction
G	Ring end-gap in its free state
h	Film thickness
h_0	Minimum film thickness
I	Second area moment of inertial of ring cross-section
h_t	Heat transfer coefficient of boundary layer
k_s	Thermal conductivity of solid surfaces
L	Big-end bearing width
l	Ring outer circumference
l_c	Connecting rod length
m	Effective mass of piston and proportion of connecting rod in pure translation
m_a	Mass of air
m_{fda}	Mass of expended fuel with cylinder deactivation
m_{fa}	Mass of expended Fuel under standard operation
m_{loss}	Mass of expended fuel
N	Engine speed in RPM
n	Step of iteration
p	Pressure
$\overline{p}$	Average Pressure
p_a	Asperity contact pressure
p_{atm}	Atmospheric pressure
p_c	Cavitation vaporisation pressure
P_b	Power loss of big-end bearing
P_e	Ring elastic pressure due to tension
P_g	Combustion gas pressure
P_{out}	Engine output power
P_r	Power loss from of piston ring-cylinder liner conjunction
Q	Calorific value of fuel
$\dot{Q}$	Generated rate of frictional heat
$\dot{Q}_{cv}$	Heat flow rate due to convection
$\dot{Q}_{in}$	Heat flow rate at the contact inlet
r	Journal radius
r_0	Nominal radius of the bore
r_c	Crank radius
R_e	Convective thermal resistance in lubricant flow
R_f	Conductive thermal resistance of solid boundaries (flash temperature rise)
R_l	Conductive thermal resistance for the lubricant film
R_v	Convective thermal resistance of the boundary layer
s	Ring face profile
S_f	Characteristic length
t	Time
U	Speed of entraining motion
V	Variance ratio
V_c	Piston swept volume
W_a	Load carried by the asperities
W_h	Load carrying capacity of hydrodynamic film
W	Total contact reaction
x	Direction along the ring face-width (direction of entraining motion)
x_c	Position of lubricant film rupture
Z	Pressure-viscosity index
z	Direction along the bearing-width

Greek Symbols

α	Piezo-viscous coefficient
β	Thermo-viscous coefficient
γ	Correlation length ratio
ΔU	Sliding speed
δ	Localised elastic deflection
ε	Numerical damping factor
ϕ	Connecting rod obliquity angle
φ	Bearing reaction attitude angle
φ_c	Contact flow factor
φ_s	Shear flow factor
φ_x	Pressure flow factor
$\varphi_{fp}, \varphi_{fs}, \varphi_f$	Friction flow factors

η_0	Lubricant dynamic viscosity at ambient pressure and temperature
η_e	Effective lubricant dynamic viscosity
θ_0	Initial/ambient temperature
θ_e	Effective lubricant contact temperature
θ_{s1}, θ_{s2}	Initial surface temperatures of liner and ring
ϑ	Circumferential position in bearing
κ	Average asperity tip radius
λ	Stribeck oil film parameter
ρ_a	Density of air at the inlet manifold
σ	Root mean square roughness of contiguous surfaces
ς	Boundary shear strength of surfaces
$\overline{\tau}$	Average shear stress
τ_0	Eyring shear stress
ζ	Asperity density per unit contact area
υ	Poisson's ratio
ω	Crankshaft angular velocity
ψ	Crank angle
χ	Load adjusting parameter

Abbreviations

BMEP	Brake mean effective pressure
CDA	Cylinder deactivation
RPM	Revolutions per minute
VVA	Variable valve actuation

Appendix 1. Flow factors

The flow factors used in the current study are based on those provided in Refs. [49,50].

The pressure flow factor φ_x is given as:

$$\varphi_x = 1 - 0.9e^{-0.56\lambda},\ \lambda > 0.5 \text{ and } \gamma = 1 \tag{A1-1}$$

where γ is the ratio of the roughness correlation lengths in the x and y directions, which equates to unity for an isotropic roughness.

The shear flow factor φ_s is calculated using:

$$\varphi_s = \begin{cases} 1.899\lambda^{0.98}(V_1 - V_2)e^{\left(-0.92\lambda + 0.05\lambda^2\right)}, & \lambda \le 5,\ \gamma = 1 \\ 1.126(V_1 - V_2)e^{-0.25\lambda}, & \lambda > 5,\ \gamma = 1 \end{cases} \tag{A1-2}$$

where, the parameters V_1 and V_2 are the variance ratios: $V_i = \sigma_i^2/\sigma^2, i \in 1, 2$.

The contact factor φ_c is calculated using:

$$\varphi_c = \frac{1}{2}[1 + erf(\lambda)] \tag{A1-3}$$

The shear stress factors φ_{fp}, φ_{fs} and φ_f are given by the following relationships:

$$\varphi_{fp} = 1 - 1.4e^{-0.66\lambda},\ \lambda > 0.75,\ \gamma = 1 \tag{A1-4}$$

$$\varphi_{fs} = \begin{cases} 11.1\lambda^{2.31}(V_1 - V_2)e^{\left(2.38\lambda + 0.11\lambda^2\right)}, & 0.5 < \lambda < 7,\ \gamma = 1 \\ 0, & \lambda > 7 \end{cases} \tag{A1-5}$$

$$\varphi_f = \begin{cases} \dfrac{35}{32}\xi\left\{\left(1-\xi^2\right)^3 \ln[300(1+\xi)] + \dfrac{1}{60}N\right\}, & \lambda \le 3 \\ \dfrac{35}{32}\xi\left\{\left(1-\xi^2\right)^3 \ln\left(\dfrac{\xi+1}{\xi-1}\right) + \dfrac{\xi}{15}\left[66 + \xi^2\left(30\xi^2 - 80\right)\right]\right\}, & \lambda > 3 \end{cases} \tag{A1-6}$$

where $\xi = \lambda/3$, $N = \xi\{\xi[132 + \xi(M + 345)]\} - 55$ and $M = \xi\{\xi[\xi(60 + 147\xi) - 405] - 160\}$

Appendix 2. Fuel energy calculation

According to Heywood and Welling [68], a typical 1.4 L engine has a peak output power $P_{out} = 80$ kW. For steady state highway driving, approximately 30% of this power is required. The following equation is used to characterise the fuel mass required with and without cylinder deactivation at the engine speed of 3000 rpm:

$$m_{fa} = \frac{2P_{out}m_a}{Q\rho_a V_c N\eta_v\eta_m\eta_f} \tag{A2-1}$$

where, Q, V_c and ρ_a are the calorific value of fuel, engine swept volume and density of air at the inlet manifold respectively. The values for $\eta_v$and η_m are found for similar engine configurations through tabulated data in Taylor [69]. Sandford et al. [1] show that under the currently prescribed operating conditions (BMEP = .38 MPa), a fuel economy improvement of 5% can be attained through cylinder deactivation. The fuel mass consumed in the deactivated case for the current condition can reasonably be considered to be:

$$m_{fda} = 0.95m_{fa} \tag{A2-2}$$

The percentage fuel expended through the big-end bearing and piston ring conjunctions can then be written as:

$$m_{loss} = \frac{P_r + P_b}{Qm_{fi}} \tag{A2-3}$$

where, m_{fi} is the m_{fda} or m_{fa}, as appropriate, and m_{loss} is the expended fuel mass due to friction in the studied contacts.

Table A2
Fuel mass calculations

Parameter	Value	Unit
η_v	0.8	–
η_m	0.6	–
η_f	0.25	–
ρ_a	1.225	kgm^{-3}
Q	45	$MJkg^{-1}$

References

[1] Sandford M, Allen J, Tudor R. Reduced Fuel Consumption and Emissions Through Cylinder Deactivation. Future Engine and System Technologies, vol. 5. London: IMechE Seminar Publications; 1998. p. 211–22.
[2] Kreuter P, Heuser P, Reinicke-Murmann J, Erz R, Stein P, Peter U. Meta-CVD System an Electro-Mechanical Cylinder and Valve Deactivation System. 2001. SAE Technical Paper No. 2001-01-0240.
[3] Andersson BS. Company's perspective in vehicle tribology. In: Dowson D, Taylor CM, Godet M, editors. Proc. 18th leeds-lyon sympos. Elsevier; 1991. p. 503–6.
[4] Takiguchi M, Sasaki R, Takahashi I, Ishibashi F, Furuhama S, Kai R, et al. Oil film thickness measurement and analysis of a three ring pack in an operating diesel engine. 2000. SAE Technical Paper 2000-01-1787.
[5] Furuhama S, Sasaki S. New device for the measurement of piston frictional forces in small engines. 1983. SAE Technical paper 831284.
[6] Gore M, Howell-Smith SJ, King PD, Rahnejat H. Measurement of in-cylinder friction using the floating liner principle. In: ASME 2012 internal combustion engine division spring technical conference; 2012. p. 901–6. May 6.
[7] Gore M, Theaker M, Howell-Smith S, Rahnejat H, King PD. Direct measurement of piston friction of internal-combustion engines using the floating-liner principle. Proc IMechE, Part D: J Automobile Engineering 2014;228(3):344–54.
[8] Sherrington I. Measurement techniques for piston-ring tribology. Tribol. Dyn. Engine Powertrain: Fundam. Appl. Future Trends 2010:387. Woodhead Publishing.
[9] Castleman Jr RA. A hydrodynamical theory of piston ring lubrication. J App. Phys. 1936;7(9):364–7.
[10] Eilon S, Saunders OA. A study of piston-ring lubrication. Proc IMechE 1957;171(1): 427–62.
[11] Furuhama S. A dynamic theory of piston-ring lubrication: 1st report, calculation. Bull. JSME 1959;2(7):423–8.
[12] Hamilton GM, Moore SL. Second Paper: comparison between measured and calculated thicknesses of the oil-film lubricating piston rings. Proc IMechE 1974; 188(1):262–8.
[13] Swift HW. The stability of lubricating films in journal bearings. Proc Inst Civil Eng 1932;233:267–88.
[14] Stieber W. Das-Schwimmlager: hydrodynamische Theorie des Gleitlagers. 1933. p. 106. No. V.D.I., Berlin.
[15] Ruddy BL, Dowson D, Economou PN. A theoretical analysis of the twin-land type of oil-control piston ring. J Mech Eng Sci 1981;23(2):51–62.
[16] Dowson D, Economou PN, Ruddy BL, Strachan PJ, Baker AJS. Piston ring lubrication, Part II: theoretical analysis of a single ring and a complete ring pack. Energy Conservation through fluid film lubrication technology: Frontiers in research and design 1979:23–52.
[17] D'Agostino V, Senatore A. Fundamentals of lubrication and friction of piston ring contact. In: Rahnejat H, editor. Tribology and dynamics of engine and powertrain: fundamentals, applications and future trends. Cambridge, UK: Woodhead Publishing Ltd.; 2010.
[18] Styles G, Rahmani R, Rahnejat H, Fitzsimons B. "In-cycle and life-time friction transience in piston ring–liner conjunction under mixed regime of lubrication. Int. J. Engine Research 2014;15(7):862–76.
[19] Bolander NW, Steenwyk BD, Sadeghi F, Gerber GR. Lubrication regime transitions at the piston ring-cylinder liner interface. Proc IMechE, Part J: J Engineering Tribology 2005;219(1):19–31.
[20] Morris N, Rahmani R, Rahnejat H, King PD, Fitzsimons B. The influence of piston ring geometry and topography on friction. Proc IMechE, Part J: J Engineering Tribology 2013;227(2):141–53.
[21] Dunaevsky VV. Analysis of distortions of cylinders and conformability of piston rings. STLE Tribology Trans. 1990;33(10):33–40.
[22] Mishra PC, Balakrishnan S, Rahnejat H. Tribology of compression ring-to-cylinder contact at reversal. Proc IMechE, Part J: J Engineering Tribology 2008;222(7): 815–26.
[23] Tian T, Rabute R, Wong VW, Heywood JB. Effects of Piston-Ring Dynamics on Ring/Groove Wear and Oil Consumption in a Diesel Engine. 1997. SAE Technical Paper No. 970835.
[24] Tian T. Dynamic behaviour of piston rings and their practical impact Part 2: oil transport, friction and wear of ring/liner interface and the effects of piston and ring dynamics. Proc IMechE, Part J:Engineering Tribology 2002;216:229–47.
[25] Baker CE, Theodossiades S, Rahnejat H, Fitzsimons B. Influence of in-plane dynamics of thin compression rings on friction in internal combustion engines. J Eng Gas Turbines Power 2012;134(9), 092801.
[26] Baker CE, Rahmani R, Theodossiades S, Rahnejat H, Fitzsimons B. On the effect of transient in-plane dynamics of the compression ring upon its tribological performance. J Eng Gas Turbines Power 2015;137(3), 032512.
[27] Baker CE, Rahmani R, Karagiannis I, Theodossiades S, Rahnejat H, Frendt A. Effect of compression ring elastodynamics behaviour upon blowby and power loss. 2014. SAE Technical Paper, 2014-01-1669.
[28] Rahmani R, Theodossiades S, Rahnejat H, Fitzsimons B. Transient elastohydrodynamic lubrication of rough new or worn piston compression ring conjunction with an out-of-round cylinder bore. Proc IMechE, Part J: J Engineering Tribology 2012;226(4):284–305.
[29] Namazian M, Heywood J. Flow in the piston-cylinder-ring crevices of a spark-ignition engine: effect on hydrocarbon emissions, efficiency and power. 1982. SAE Technical Paper 820088.
[30] Baker CE, Theodossiades S, Rahmani R, Rahnejat H, Fitzsimons B. On the transient three dimensional tribodynamics of internal combustion engine top compression ring. J Eng Gas Turbines Power 2017;139(6), 062801.
[31] Sui PC, Ariga S. Piston ring pack friction and lubrication analysis of an automotive engine using a mixed lubrication model. 1993. SAE Technical Paper No.931937.
[32] Ma Z, Henein NA, Bryzik W. A model for wear and friction in cylinder liners and piston rings. Tribol Trans 2006;49:315–27.
[33] Morris N, Rahmani R, Rahnejat H, King PD, Fitzsimons B. Tribology of piston compression ring conjunction under transient thermal mixed regime of lubrication. Tribol Int 2013;59:248–58.
[34] Rahmani R, Rahnejat H, Fitzsimons B, Dowson D. The effect of cylinder liner operating temperature on frictional loss and engine emissions in piston ring conjunction. Appl Energy 2017;191:568–81.

[35] Ma MT, Smith EH, Sherrington I. Analysis of lubrication and friction for a complete piston-ring pack with an improved oil availability model: Part 2: circumferentially variable film. Proc IMechE, Part J: J Engineering Tribology 1997;211(1):17–27.
[36] Mishra PC, Rahnejat H, King PD. Tribology of the ring-bore conjunction subject to a mixed regime of lubrication. Proc IMechE, Part C: J Mech Eng Science 2009;223(4):987–98.
[37] Bewsher SR, Turnbull R, Mohammadpour M, Rahmani R, Rahnejat H, Offner G, et al. Effect of cylinder de-activation on the tribological performance of compression ring conjunction. Proc IMechE, Part J: J Eng Tribology 2017;231(8):997–1006.
[38] Martin FA, Booker JF. Influence of engine inertia forces on minimum film thickness in con-rod big-end bearings. Proc IMechE 1966;181(1):749–64.
[39] Booker JF. Dynamically-loaded journal bearings: numerical application of the mobility method. Trans. ASME, J. Lubr. Tech. 1971;93(1):168–74.
[40] Boedo S. Practical tribological issues in big end bearings. In: Tribology and dynamics of engine and powertrain. Cambridge: Woodhead Publishing; 2010. p. 615–35.
[41] Bates TW, Fantino B, Launay L, Frêne J. Oil film thickness in an elastic connecting-rod bearing: comparison between theory and experiment. Tribol Trans 1990;33(2):254–66.
[42] Rahnejat H. Multi-body dynamics: historical evolution and application. Proc IMechE, Part C: J Mech Eng Science 2000;214(1):149–73.
[43] Balakrishnan S, McMinn C, Baker CE, Rahnejat H. Fundamentals of crank and camshaft support journal bearings. In: Rahnejat H, editor. Tribology and dynamics of engine and powertrain. Cambridge, UK: Woodhead Publishing; 2010.
[44] Mishra PC, Rahnejat H. Tribology of big end bearings. In: Rahnejat H, editor. Tribology and dynamics of engine and power train. Cambridge, UK: Woodhead Publishing; 2010.
[45] Wang D, Parker DD. Effects of crank-pin surface circumferential waviness on the EHL of a big-end bearing in a diesel engine. 2003. SAE Technical Paper, No. 2003-01-3120.
[46] Bonneau D, Guines D, Frene J, Toplosky J. EHD analysis, including structural inertia effects and a mass-conserving cavitation model. Trans. ASME, J. Tribology 1995;117(3):540–7.
[47] Shahmohamadi H, Rahmani R, Rahnejat H, Garner CP, Dowson D. Big end bearing losses with thermal cavitation flow under cylinder deactivation. Tribol Lett 2015;57(1):2.
[48] Mohammadpour M, Rahmani R, Rahnejat H. Effect of cylinder deactivation on the tribo-dynamics and acoustic emission of overlay big end bearings. Proc IMechE, Part K: J Multi-body Dynamics 2014;228(2):138–51.
[49] Patir N, Cheng HS. An average flow model for determining effects of three-dimensional roughness on partial hydrodynamic lubrication. Trans. ASME, J. lubrication Technology 1978;100(1):12–7.
[50] Chengwei W, Linqing Z. An average Reynolds equation for partial film lubrication with a contact factor. Trans. ASME, J. Trib. 1989;111:188–91.
[51] Haddad SD, Tjan K-T. An analytical study of offset piston and crankshaft designs and the effect of oil film on piston slap excitation in a diesel engine. Mech Mach Theor 1995;30(2):271–84.
[52] Houpert L. New results of traction force calculations in elastohydrodynamic Contacts. Trans. ASME, J. Tribology 1985;107(2):241–5.
[53] Dowson D, Higginson GR. Elasto-hydodynamic lubrication. 2nd SI edition. Oxford: Pergamon Press; 1977.
[54] Tian T, Noordzij L, Wong VW, Heywood JB. Modeling piston-ring dynamics, blowby, and ring-twist effects. J Eng Gas Turbines Power 1998;120(4):843–54.
[55] Theaker M, Rahmani R, Rahnejat H. Prediction of ring-bore conformance and contact condition and experimental validation. In: ASME international engine division spring technical conference; 2012. paper number: ICES2012–81021, May 6-9, Torino, Italy.
[56] Greenwood JA, Tripp JH. The contact of two nominally flat rough surfaces. Proc. IMechE, J. Mech. Eng. Sci. 1970-71;185(1):625–33.
[57] Leighton M, Morris N, Gore M, Rahmani R, Rahnejat H, King PD. Boundary interactions of rough non-Gaussian surfaces. Proc IMechE, Part J: J Engineering Tribology 2016;230(11):1359–70.
[58] Briscoe BJ, Evans DC. The shear properties of Langmuir-Blodgett layers. Proc Math Phys Eng Sci 1982;380(1779):389–407.
[59] Teodorescu M, Balakrishnan S, Rahnejat H. Integrated tribological analysis within a multi- physics approach to system dynamics. Trib. & Interface Sci. Series 2005;48:725–37.
[60] Sharif KJ, Evans HP, Snidle RW, Newall JP. Modeling of film thickness and traction in a variable ratio traction drive rig. Trans. ASME, J. Trib 2004;126:92–104.
[61] Carslaw HS, Jaeger JC. Conduction of heat in solids. second ed. Oxford, UK: Oxford Science Publications; 1959.
[62] Gore M, Rahmani R, Rahnejat H, King PD. Assessment of friction from compression ring conjunction of a high-performance internal combustion engine: a combined numerical and experimental study. Proc IMechE, Part C: J Mechanical Engineering Science 2016;230(12):2073–85.
[63] Rahnejat H. Multi-body dynamics: vehicles, machines and mechanisms. UK: Professional Engineering Publishing, Bury St Edmunds; 1998.
[64] Etsion I, Sher E. Improving fuel efficiency with laser surface textured piston rings. Tribol Int 2009;42(4):542–7.
[65] Etsion I. Surface texturing for in-cylinder friction reduction. New Delhi (India): Woodhead Publishing Ltd; 2010.
[66] Morris NJ, Rahmani R, Rahnejat H. A hydrodynamic flow analysis for optimal positioning of surface textures. Proc IMechE, Part J: J Engineering Tribology 2017;231(9):1140–50.
[67] Morris N, Rahmani R, Rahnejat H, King PD, Howell-Smith S. A numerical model to study the role of surface textures at top dead center reversal in the piston ring to cylinder liner contact. Trans. ASME, J. Tribology 2016;138(2), 021703.
[68] Heywood JB, Welling OZ. Trends in performance characteristics of modern automobile SI and diesel engines. SAE Int. J. Engines 2009;2(2009–01-1892):1650–62.
[69] Taylor CF. The internal-combustion engine in theory and practice. MIT press; 1985.
[70] McClure F. Numerical modeling of piston secondary motion and skirt lubrication in internal combustion engines. Doctoral dissertation. Massachusetts Institute of Technology; 2007.
[71] Littlefair B, De la Cruz M, Theodossiades S, Mills R, Howell-Smith S, Rahnejat H, et al. Transient tribo-dynamics of thermo-elastic compliant high-performance piston skirts. Tribol Lett 2014;53(1):51–70.